Migration of Seismic Data

JENÖ GAZDAG AND PIERO SGUAZZERO

Invited Paper

Reflection seismology seeks to determine the structure of the earth from seismic records obtained at the surface. The processing of these data by digital computers is aimed at rendering them more comprehensible geologically. Seismic migration is one of these processes. Its purpose is to "migrate" the recorded events to their correct spatial positions by backward projection or depropagation based on wave theoretical considerations. During the last 15 years several methods have appeared on the scene. The purpose of this paper is to provide an overview of the major advances in this field. Migration methods examined here fall in three major categories: 1) integral solutions, 2) depth extrapolation methods, and 3) time extrapolation methods. Within these categories, the pertinent equations and numerical techniques are discussed in some detail. The topic of migration before stacking is treated separately with an outline of two different approaches to this important problem.

I. Introduction

The purpose of migration is to reconstruct the reflectivity map of the earth from the seismic data recorded at the surface. The seismic signal recorded by a receiver (geophone) is a superposition of seismic waves originating from all possible directions in the subterrain. Thus the recorded events most often are not from reflectors directly below the receiver but from geological formations far away from the point of recording. The term *migration* refers to the movement of the observed events to their true spatial positions. Migration is an inverse process, in which the recorded waves are propagated back to the corresponding reflector locations. The concept of migration can be summarized in the following terms. In the process of seismic data acquisition the upward traveling waves are recorded at the surface. In the migration process these recorded waves are used either as initial conditions or boundary conditions for a wavefield governed by the wave equation. As a result, these waves are propagated *backward* and in *reverse time*, from the surface to the reflector locations.

Until the 1960s, migration was achieved by graphical methods. This was followed by diffraction summation and wavefront migration based on ray theoretical considerations. In the 1970s, several important developments took place. Based on the pioneering work of Jon Claerbout, migration methods based on wave theory were developed. Efficient algorithms developed from simplified finite-difference approximations of the wave equations for downward extrapolation. Another important processing advance was made by the introduction of Fourier transform methods. These frequency-domain approaches proved to be more accurate than finite-difference methods in the space–time coordinate frame. At the same time, the diffraction summation migration was improved and modified on the basis of the Kirchhoff integral representation of the solution of the wave equation. The resulting migration procedure, known as Kirchhoff migration, compares favorably with other methods. A relatively recent advance is represented by reverse-time migration, which is related to wavefront migration.

The aim of this paper is to present the fundamental concepts of migration. While it represents a review of the state of the art, it is intended to be of tutorial nature. The reader is assumed to have no previous knowledge of seismic processing. However, some familiarity with Fourier transforms and their applications is assumed. The organization of the paper is as follows. First, the basic concepts of seismic data representation are introduced. Next, migration schemes based on integral or summation methods are discussed. Section IV deals with the derivation of the one-way wave equations. This is followed by the numerical aspects of migration methods. Migration in object space, known as reverse-time migration, is presented in Section VI, and Section VII is devoted to migration before stacking.

The effect of migration on a seismic section depends on the velocity and the reflectivity structure of the subterrain. Flat, horizontal reflectors in a medium that has no significant velocity variations may not need to be migrated. On the other hand, seismic sections from media having steeply dipping reflectors and strong lateral velocity variations need to be migrated for correct interpretation. In the latter case, migration can have a profound impact on the image, as we shall see in the example of model 2 (Figs. 11–14) to be discussed in Section V.

II. Representation of Seismic Data

A. Data Acquisition

Reflection seismology is an echo-ranging technique. An acoustic source (shot) emits a short pulse and a set of recorders (geophones) register the reflected waves at the surface. The time series (sampled) data associated with a single shot and receiver is known as a trace. In typical marine exploration (Fig. 1), a boat tows a source and a streamer of receivers. As it moves one-half receiver interval along a seismic line, it fires a shot and records the pressure at each receiver location. A trace is associated with each shot and receiver point.

Let r be the horizontal coordinate of the receiver and s be the horizontal coordinate of the source. Both are mea-

Manuscript received May 3, 1984; revised May 16, 1984.
J. Gazdag is with IBM Scientific Center, Palo Alto, CA 94304, USA.
P. Sguazzero is with IBM Scientific Center, 00149 Rome, Italy.

0018-9219/84/1000-1302$01.00

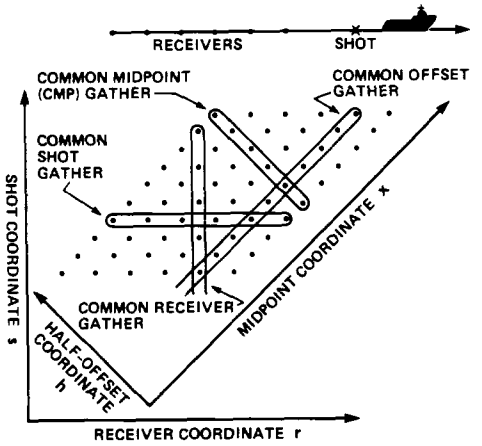

Fig. 1. Relationship among the horizontal coordinates r, s, x, and h. All axes represent distances measured along the seismic line. Each dot on the surface corresponds to a seismic trace.

sured along the seismic line. However, for mathematical reasoning, it is helpful to represent the receiver coordinate r and the source coordinate s on orthogonal axes, as shown in Fig. 1. We also define the midpoint coordinate between source and receiver as $x = (r + s)/2$, and the source/receiver half-offset coordinate as $h = (r - s)/2$. From these equations we see that x and h are another set of axes rotated 45° with respect to the axes r and s.

To understand the reason for migration let us consider the ray paths associated with two point reflectors shown in Fig. 2. Each trace includes two wavelets at times t measured

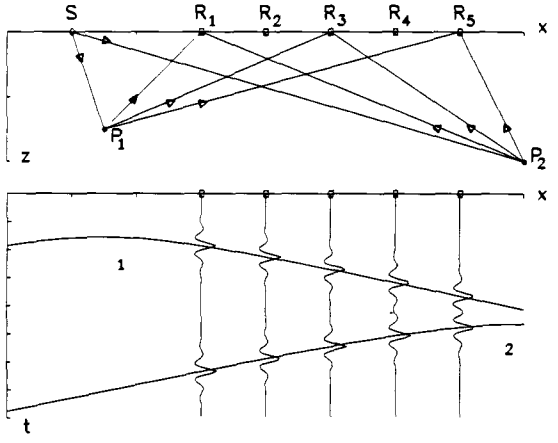

Fig. 2. The seismic concept illustrated with two point reflectors. The recorded traces form a common-shot gather. The loci of the recorded wavelets represent two-way travel time as indicated.

along the raypaths from source to object and from there to the receiver. This example clearly demonstrates that a trace consists of a superposition of seismic waves propagating from all possible directions. Consequently, the information regarding the cross section of reflectivity must be inferred from the interrelationships among an ensemble of traces. To do this, we need efficient and accurate computational techniques to map the wavelets onto the location of the reflecting objects. This mapping can also be viewed as a reconstruction of the wavefield at the time when the reflection took place. In this process, wave energy is being "migrated" over the (r, s) plane shown in Fig. 1.

For practical and economical reasons, conventional seismic processing techniques have been developed for groups of traces, called gathers, aligned parallel with one of the four axes shown in Fig. 1. A set of traces with the same source (s = constant) form a common-shot gather. The traces are also rearranged into common-midpoint (CMP) gathers or common-offset gathers as shown in Fig. 1. The reason is that the two standard operations that are responsible for the transferring of wave energy to its proper position are *stacking* of the CMP gathers and *migration* of the resulting stacked CMP section. Stacking shifts energy with respect to the offset axis, and migration shifts energy with respect to the midpoint axis. The reason for performing these operations separately is economic. Ideally, they should be performed together as discussed in Section VII.

B. Stacking

Stacking consists of the summation of the traces of each CMP gather after correcting them to compensate for the offset between source and receiver. This is known as the normal moveout (NMO) correction. The NMO process is illustrated on the idealized model shown in Fig. 3. The

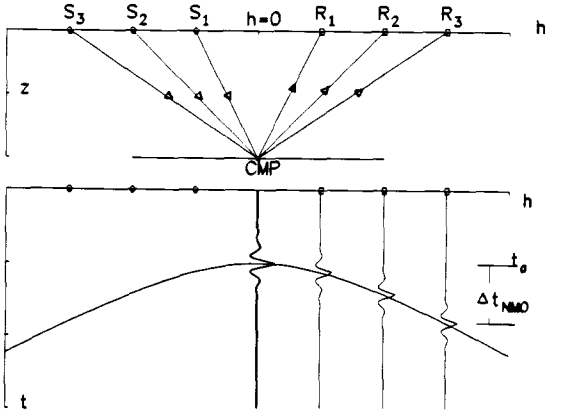

Fig. 3. Illustration of NMO correction and stacking. The traces of the CMP gather are summed along the NMO hyperbola as indicated. The normalized stacked trace is plotted at $h = 0$.

wavelets indicate reflected events from the horizontal plane. Their two-way travel time is given by

$$t^2(h) = t_0^2 + \frac{4h^2}{v^2} \tag{1}$$

assuming that the velocity of wave propagation v is constant. This equation is the NMO hyperbola. The difference between the reflection time observed for an offset $2h$ and that corresponding to $h = 0$ is the NMO correction, i.e.,

$$\Delta t_{NMO} = t(h) - t_0. \tag{2}$$

When this amount of time shift is applied to the wavelets shown in Fig. 3, apart from a minor distortion effect, they appear as if they were recorded with coincident source and receiver, i.e., $h = 0$. The NMO corrected traces are then summed, or stacked. The ensemble of stacked traces along

the midpoint axis is referred to as the CMP stacked section. A very important benefit of this operation is the significant improvement in the signal-to-noise ratio of the CMP section in comparison with the unstacked data.

C. The Exploding Reflector Model

A CMP section may be regarded as data obtained from coincident sources and receivers ($h = 0$), as shown in Fig. 4(a). In this zero-offset model, the energy travel path from source to reflector is identical to that from reflector to

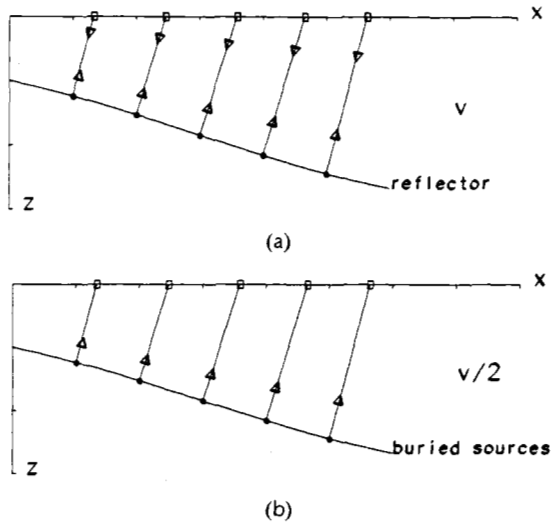

Fig. 4. (a) The CMP section may be regarded as data obtained with coincident (zero-offset) sources and receivers. (b) The exploding reflector model of the CMP data for migration.

receiver. The assumption is that all sources are activated simultaneously, but each receiver records signals originating from the same source–receiver point.

Such zero-offset data do not correspond to any wavefield resulting from a single experiment. As a result, it is helpful to create a hypothetical physical experiment to provide an intuitive picture of zero-offset migration. Such an experiment is known as the "exploding reflector model" [1]. In this model, shown in Fig. 4(b), the energy sources are not at the surface, but they are distributed along the reflecting surfaces. In other words, the reflectors are represented by buried sources, which are activated at the same time $t = 0$. Therefore, one needs to be concerned only with upward traveling waves. Since the record section involves *two-way* travel time, it needs to be converted to *one-way* travel time. In practice, the time scale of CMP sections is kept unchanged. Instead, the velocity of wave propagation is scaled down by a factor of two.

III. Integral Methods for Migration of CMP Data

With the help of the exploding reflector model outlined above, migration of CMP data can be defined as the mapping of the wavefields recorded at the surface back to their origin at $t = 0$. The basic theory of wavefield reconstruction is due to Hagedoorn [2]. Based on his ideas, graphical methods were developed, which were later implemented on digital computers. Our objective is to describe two simple classical methods followed by that of the Kirchhoff method, which is based on an integral representation of the solution of the wave equation. First, however, a geometric view of wavefield reconstruction is studied in some detail, though at an introductory level. Our guiding principle is to convey the concepts of migration in a simple descriptive manner. The specific techniques used to implement these ideas in the form of practical and efficient computer programs are not considered in this paper.

A. Geometric View of Wave Reconstruction

Let us consider the space–time distribution of energy in a simple seismic experiment shown in Fig. 5. The (x, z) *object plane* represents the cross section of the earth, and the (x, t) *image plane* is the record section. In the example shown, there is one point diffractor in the object plane. When such a point diffractor is excited by a surface source, it sets off outgoing waves in all directions. Using the exploding reflector model, such a diffractor can be approximated by a buried point source. Using $v/2$ as the velocity

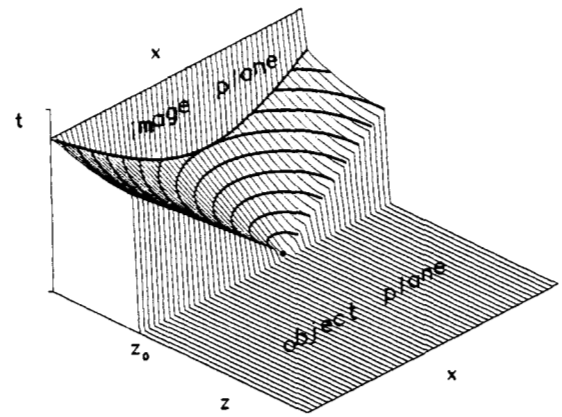

Fig. 5. The space–time distribution of the energy of a point source activated at $t = 0$ forms a cone. The intersection of this cone with the image plane $z = 0$ defines the diffraction hyperbola.

of wave propagation, the waves observed and recorded at $z = 0$ result in a zero-offset image of the diffractor.

Assuming that $v =$ constant, after the point source is set off at $t = 0$, the resulting wavefronts are concentric circles, which expand with increasing time, as shown in Fig. 5. From this diagram it is seen that the space–time (x, z, t) distribution of the wave energy lies on a cone. The intersection of this cone with the $z = 0$ plane is a hyperbola expressed by

$$t = \frac{2}{v}\left(z_0^2 + x^2\right)^{1/2}. \tag{3}$$

The upward propagating part of the energy from the point source lies along a hyperbola in the record section. The objective of migration is to recreate from the observed data in the image plane the situation that existed in the object plane at $t = 0$. In other words, migration may be regarded as a procedure of mapping the wave energy distributed along diffraction hyperbolas into the loci of the corresponding point sources.

Another way to establish the relationship between the recorded image and the object it represents is to examine the significance of a point, say a delta function, in the

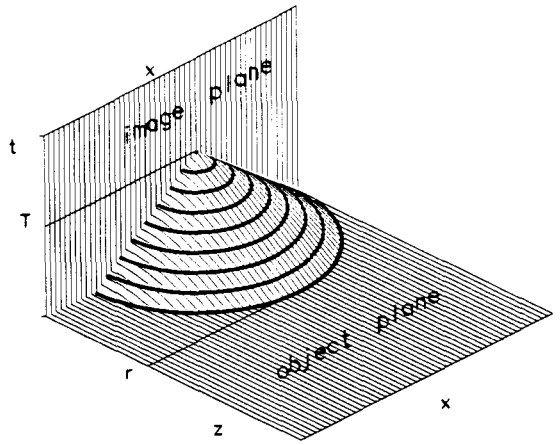

Fig. 6. The space–time distribution of the energy of an inward propagating circular wavefront (centered at $z = 0$) lies on a cone. At time T all the energy is focused in the neighborhood of a point. The reverse of this process forms the basis of wavefront migration.

image space. Consider the half-circle centered at $z = 0$ shown in Fig. 6. The initial conditions at $t = 0$ are arranged so that the acoustic energy distributed uniformly along the half-circle propagates inward, forming smaller concentric semicircles, until at $t = T$ the energy is focused in one point. Thus the energy observed at some $t = T$ on the image plane may be thought of as being originated from a wavefront lying on a half-circle centered at $z = 0$ and having a radius $r = vT/2$, as shown in Fig. 6. Consequently, in the process of reconstructing the wavefront of $t = 0$, a point of the image plane must be mapped onto a half-circle in the object plane. This means that a point diffractor in the subsurface would cause a hyperbolic seismic event, but a point on a seismic section must have been caused by a half-circle reflector in the subsurface.

B. Classical Methods of Migration

We have seen that for a constant-velocity medium the zero-offset record section of a point reflector is characterized by a diffraction hyperbola. Thus to account for all the energy due to the point source in estimating its intensity, we perform the following summation. For each (x, z) point of the object plane, we construct a diffraction hyperbola in the image plane. We determine where the hyperbola intersects each trace. Then we take the value of each trace at the point of intersection and sum all these values together. The result of this summation is taken as the value of the migrated section at (x, z), and this value is placed in the object plane at that point. This method is called *diffraction summation* (or *diffraction stack*) *migration* and represents a straightforward, albeit not theoretically sound, approach. Fig. 7 shows how, in diffraction summation migration, an output trace is generated from the input traces. The input traces represent the stacked section, whereas the output traces define the depth section.

It should be noted that, in practice, depth is most often measured in units of the two-way vertical travel time, $\tau = 2z/v$. Under the constant velocity assumption, τ corresponds to the apex of the diffraction hyperbola. Thus diffraction summation migration amounts to summing wave amplitudes along the diffraction hyperbola and mapping the result at the apex of the same hyperbola.

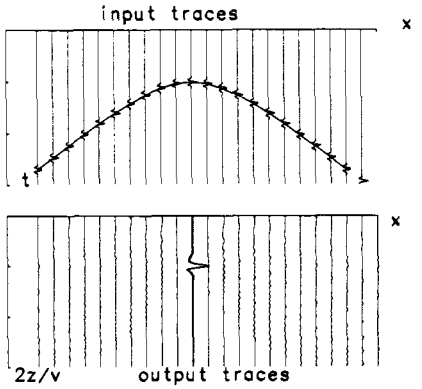

Fig. 7. Diffraction summation migration. The input traces are summed along the diffraction hyperbola corresponding to a single scatterer at location x to produce an output trace at each location x.

A counterpart of diffraction migration is *wavefront interference migration*, which can be understood from the geometrical view shown in Fig. 6. This approach to migration is based on the observation that each point in the image plane must be mapped into a semi-circle in the object plane. Thus the wavefront method [3] is a "one to many" mapping. For the constant velocity case, the procedure is the following. We take a sample of a seismic trace in the record section and distribute it over a semi-circle (equal travel times) in the object plane as illustrated in Fig. 8.

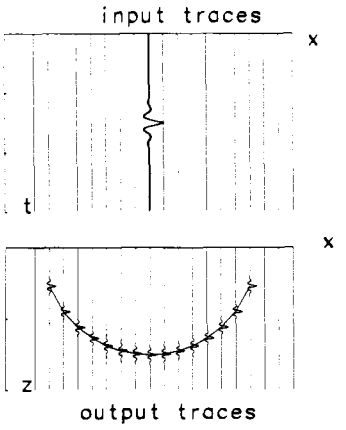

Fig. 8. Wavefront migration. Each input trace is mapped onto a semi-circle corresponding to the proper wavefront.

The diffraction summation and the wavefront interference methods had notable success in the late 1960s and early 1970s [4]. They also have a number of undesirable characteristics [3, p. 124]. The reason for their shortcomings is rooted in the fact that while these migration procedures make good sense and are intuitively obvious, they are not based on a completely sound theory.

C. The Kirchhoff Method

The Kirchhoff integral theorem expresses the value of the wavefield at an arbitrary point in terms of the value of the wavefield and its normal derivative at all points on an arbitrary closed surface surrounding the point [5, p. 377]. In practice, measurements are made only at the surface, therefore, instead of a closed surface, the integration must be

limited to the surface of the earth. Furthermore, in seismic practice, only the wavefield is recorded, and its normal derivative is not available. The Kirchhoff integral can be expressed more easily for three-dimensional data, i.e., where the pressure wavefield is defined over some area of the earth's surface rather than along a line as we assumed in the two-dimensional case. Let $p(x, y, z = 0, t)$ be the recorded data, where x and y are surface coordinates, z is depth, and t is time. Then the migrated wavefield at some point (x_1, y_1, z_1, t) is obtained from the following expression [6], [7], [8, p. 125], [9], as:

$$p(x_1 y_1, z_1, t = 0) = \int\int \frac{\cos\vartheta}{2\pi rc} \frac{\partial p}{\partial t}(x, y, z = 0, t = r/c)\, dx\, dy \quad (4)$$

where

$$r = \left[(x_1 - x)^2 + (y_1 - y)^2 + z_1^2\right]^{1/2}$$

$c = v/2$ is the half velocity (assuming that t is the two-way travel time), and ϑ is the angle between the z axis and the line joining (x_1, y_1, z_1) and $(x, y, z = 0)$.

To obtain the two-dimensional version of (4), one must assume that p is independent of y. After integrating with respect to y, one obtains the following asymptotic approximation [8, p. 126]:

$$p(x_1, z_1, t = 0) = \int \frac{\cos\vartheta}{\sqrt{2\pi rc}} \partial_t^{1/2} p(x, z = 0, t = r/c)\, dx \quad (5)$$

where $\partial_t^{1/2}$ denotes the *half derivative* with respect to t. A simple expression for the operator $\partial_t^{1/2}$ can be given in the frequency domain, where the transfer function of $\partial_t^{1/2}$ is given by

$$D^{1/2}(\omega) = (i\omega)^{1/2} = \sqrt{\omega}\, \exp(i\pi/4). \quad (6)$$

It should be observed that, apart from the half-derivative operator and a weighting factor, (5) represents an integration along the diffraction hyperbola. In this respect it is quite similar to the diffraction summation method. It is important to note, however, that the Kirchhoff method yields significantly higher quality migration than the diffraction summation approach discussed earlier.

When the propagation velocity c varies with the space coordinates x, y, and z, (4) and (5) must be suitably generalized. For instance, in two dimensions we obtain [10]

$$p(x_1, z_1, t = 0) = \int W \partial_t^{1/2} p(x, z = 0, t = T(x_1, z_1, x, z = 0))\, dx \quad (7)$$

where W is a weighting factor, and $T(x_1, z_1, x, z)$ represents the two-way travel time measured along a raypath that connects the points (x_1, z_1) and (x, z) obeying Fermat's least time principle [5, p. 128].

D. Synthetic Seismic Records

As we have discussed earlier, migration is an inverse process. To test a migration scheme and evaluate its performance, we need a set of seismic data, e.g., a zero-offset section obtained from an idealized model with known reflectivity and velocities. This is usually done by simulating the forward process, collecting the results into traces, and arranging these traces into some kind of gathers or constant-offset sections. The computer generation of seismic data calls for the solution of the equations governing the wave propagation in the medium defined in the model under consideration. It is important, however, to ensure that the modeling is not simply an inverse of the migration from the numerical and algorithmic point of view. Otherwise, errors in the forward process may be partially canceled in the inverse process, which can lead to incorrect error estimates. To avoid these pitfalls, the synthetic seismic records presented in this paper are obtained by means of an algorithm that permits the computation of two-way reflection times with precision limited only by roundoff error.

In our approach to forward modeling, the reflecting objects are represented by scattering surfaces in three dimensions, or lines in two dimensions. The utility of approximating a continuous reflecting sheet by discrete scattering points in a scaled seismic test tank was shown by Gardner *et al.* [11]. The computer implementation of this method is based upon the ray theory of diffraction and the superposition principle. The modeling of a complex subsurface reflectivity structure is done by representing it as a set of independent point scatterers. To obtain the zero-offset section of an elementary diffractor, following the exploding reflector principle, rays are traced in every direction through the medium up to the surface. A wavelet whose amplitude is proportional to the strength of the diffractor is assigned (after taking into account geometrical spreading) to the grid point of the time section corresponding to the arrival of the ray at the surface. The contributions of all point diffractors are then summed to obtain the zero-offset section of the structure.

An example of this modeling approach is Model 1 representing a syncline shown in Fig. 9(a). The synthetic zero-offset section of Model 1 is shown in Fig. 9(b), assuming a uniform velocity of $v = 3$ km/s. Fig. 10 illustrates the same

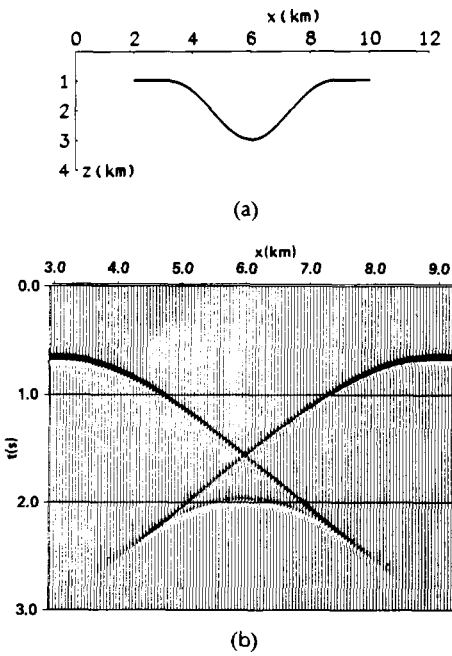

Fig. 9. (a) Schematic of Model 1, representing a syncline in a constant velocity medium. (b) Synthetic zero-offset time section of Model 1.

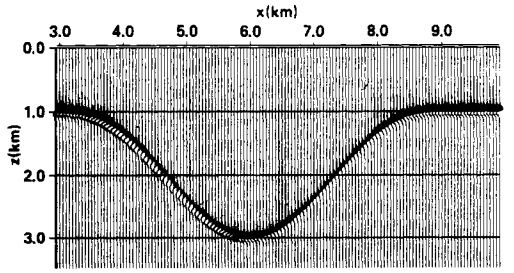

Fig. 10. Migrated section obtained from the zero-offset section of Model 1 (Fig. 9(b)) by means of the Kirchhoff method.

section after migration using the Kirchhoff summation method. We note that all the wave energy is distributed along the syncline, which demonstrates the high accuracy that can be expected from the Kirchhoff migration expressed by (4) and (5).

IV. Wave-Equation Migration in Image Space

Since we are dealing with wave phenomena, as one can reasonably expect, migration can also be described as a method of obtaining the numerical solution of some partial-differential equation. These partial-differential equations can be solved numerically either in the *image space* or in the *object space*. For historical and practical reasons, migration schemes formulated in image space are considerably more popular than those defined in object space. A variety of migration techniques based on solving a wave equation over a computational grid in image space has evolved in the last decade or so. These methods are generally referred to as *wave-equation migration*. This name can be misleading since it seems to suggest that the Kirchhoff method is not based on wave theory. To be sure, all migration methods with solid theoretical foundation must be, by definition, wave-equation methods.

In what follows we shall derive the equations for wave extrapolation under the simplifying assumption that the velocity of the medium has no lateral dependence. The treatment of laterally varying media will be presented in the latter part of the paper. The equations under consideration are for extrapolation of seismic data obtained from multiple sources and multiple recorders as illustrated in Fig. 1.

A. Equations for Wavefield Extrapolation

We shall follow the notation used in describing the data acquisition illustrated in Fig. 1. We let r and s be the horizontal coordinates of the receiver and the source, respectively. We also define the midpoint coordinate $x = (r + s)/2$ and the half-offset $h = (r - s)/2$. The variable z represents depth into the ground. We let $p(r, s, t, z_r, z_s)$ represent the wavefield, where z_r and z_s are depth coordinates for recorder and sources, respectively. For fixed sources, the waves seen by the recorders are governed by the scalar wave equation

$$\frac{\partial^2 p}{\partial t^2} = v^2\left[\frac{\partial^2 p}{\partial r^2} + \frac{\partial^2 p}{\partial z_r^2}\right] \tag{8}$$

in which v stands for the velocity of wave propagation. The reciprocity principle permits the interchange of sources and receivers. Using this principle and fixing the receivers we can express the behavior of the waves in terms of the source coordinates as

$$\frac{\partial^2 p}{\partial t^2} = v^2\left[\frac{\partial^2 p}{\partial s^2} + \frac{\partial^2 p}{\partial z_s^2}\right]. \tag{9}$$

Assuming that the velocity function has no lateral variations, that is, it does not depend on r and s, we may Fourier-transform (8) and (9) with respect to r, s, and t. This operation gives

$$\frac{\partial^2 P}{\partial z_r^2} = -\left(\frac{\omega}{v}\right)^2\left[1 - \left(k_r\frac{v}{\omega}\right)^2\right]P \tag{10}$$

and

$$\frac{\partial^2 P}{\partial z_s^2} = -\left(\frac{\omega}{v}\right)^2\left[1 - \left(k_s\frac{v}{\omega}\right)^2\right]P \tag{11}$$

where k_r and k_s are the wavenumbers (or spatial frequencies) with respect to r and s, respectively, and ω is the temporal frequency. $P(k_r, k_s, \omega, z_r, z_s)$ is the Fourier transform of $p(r, s, t, z_r, z_s)$.

Equations (10) and (11) have two independent solutions that propagate in opposite senses in (r, s, t) space. One moves in the positive t-direction, the other in the negative t-direction. These pairs of solutions are generally referred to as upgoing and downgoing waves [12, p. 169], [13, p. 428]. We reconstruct the wavefield by lowering the source and recorder coordinates to the location of a reflector under consideration [14]. Coincident source and recorder positions imply $t = 0$. Therefore, the only meaningful solution is the one that returns to zero time, the one that represents regressing waves when moving downward. The one-way wave equations that govern these regressive waves are

$$\frac{\partial P}{\partial z_r} = \frac{i\omega}{v}\left[1 - \kappa_r^2\right]^{1/2}P \tag{12}$$

and

$$\frac{\partial P}{\partial z_s} = \frac{i\omega}{v}\left[1 - \kappa_s^2\right]^{1/2}P \tag{13}$$

where we have introduced

$$\kappa_r = \frac{k_r v}{\omega} \quad \text{and} \quad \kappa_s = \frac{k_s v}{\omega} \tag{14}$$

to simplify the notation.

When recorders and sources are lowered simultaneously, their position may be denoted by a common depth coordinate z, i.e., one may let

$$z_r = z \quad \text{and} \quad z_s = z. \tag{15}$$

This permits us to write

$$\frac{\partial P}{\partial z} = \frac{\partial P}{\partial z_r} + \frac{\partial P}{\partial z_s}. \tag{16}$$

Substituting (12) and (13) into (16) we obtain

$$\frac{\partial P}{\partial z} = \frac{i\omega}{v}\left\{\left[1 - \kappa_r^2\right]^{1/2} + \left[1 - \kappa_s^2\right]^{1/2}\right\}P \tag{17}$$

which expresses the simultaneous downward extrapolation of recorders and sources. This expression is known as the *double-square-root equation* [15]. The solution of (17) can be expressed as

$$P(z+\Delta z) = P(z)\exp\left\{\frac{i\omega}{v}\left[\left(1-\kappa_r^2\right)^{1/2} + \left(1-\kappa_s^2\right)^{1/2}\right]\Delta z\right\}. \quad (18)$$

If the data are defined in the (x, h) domain, it is desirable to express κ_r and κ_s as functions of k_x and k_h, which are the wavenumbers with respect to x and h, respectively. Using the relationship among receiver and source coordinates r and s, and midpoint and half-offset coordinates x and h, that is

$$x = (r+s)/2 \qquad h = (r-s)/2 \quad (19)$$

we find

$$\kappa_r = \frac{(k_x + k_h)v}{2\omega} \quad \text{and} \quad \kappa_s = \frac{(k_x - k_h)v}{2\omega}. \quad (20)$$

Once the surface data have been extrapolated by means of (18) to the entire half-space $z > 0$, migration can be accomplished by imaging the wavefield at $t = 0$, $r = s$. Thus the correctly migrated zero-offset data are given by

$$p(x, h=0, t=0, z) = \sum_{k_x}\sum_{k_h}\sum_{\omega} P(k_x, k_h, \omega, z)\exp(ik_x x). \quad (21)$$

B. Wave Equation for Zero-Offset Data

In current seismic practice, chiefly for economic reasons, migration is performed after NMO and stacking on CMP sections. The NMO correction transforms data into zero-offset under the assumption that

$$p(x, h, t', z=0) \cong p(x, h=0, t, z=0) \quad (22)$$

in which t' differs from t by the amount of the NMO correction, i.e.,

$$t' = t + \Delta t_{\mathrm{NMO}} \quad (23)$$

where Δt_{NMO} is defined by (2) and illustrated in Fig. 3. If we let $\tilde{p}$ denote the NMO corrected version of p, then in view of (22), $\tilde{p}$ can be regarded as being independent of h

$$\tilde{p}(x, h, t, z=0) \cong p(x, h=0, t, z=0). \quad (24)$$

Therefore, its Fourier transform is zero for all nonzero wavenumbers k_h, i.e.,

$$\tilde{P}(k_x, k_h, \omega, z=0) \cong 0, \qquad \text{for } k_h \neq 0. \quad (25)$$

Note that (17) is still the correct extrapolation equation for $\tilde{P}$. Substituting (20) into (17) and using (25) we obtain

$$\frac{\partial \tilde{P}}{\partial z} = \frac{2i\omega}{v}\left[1-\left(\frac{k_x v}{2\omega}\right)^2\right]^{1/2}\tilde{P}. \quad (26)$$

The one-way wave equation (26) is the fundamental equation for downward extrapolation of zero-offset data. It is expressed in the wavenumber–frequency domain (k_x, ω), and does not have an explicit representation in the midpoint-time domain (x, t). We have obtained it as a special case of a general extrapolation equation for multioffset data. It can also be easily derived by making use of the exploding reflector model of zero-offset data as shown elsewhere [16], [19]. It should be observed that the velocity variable that figures in (26) is the half velocity, as one would expect, from the exploding reflector model for zero-offset data.

V. Numerical Methods for Zero-Offset Migration in Image Space

Migration of zero-offset seismic data in image space can be summarized as follows. The zero-offset data are extrapolated from the surface downward to some depth $z = n\Delta z$ in n computational steps. The wave extrapolation calls for the numerical solution of (26) or some approximation thereof. The computations are performed in the *image space*, using the zero-offset section as initial condition. In this process, as z increases, recorded events are shifted laterally toward thier correct position as they move in the negative t direction. Downward extrapolation to depth z results in a wavefield that would have been recorded, if both sources and recorders had been located at depth z. Thus events appearing at $t = 0$ are at their correct lateral position. Therefore, the extrapolated zero-offset data at $t = 0$ are taken as being the correctly migrated data at the current depth. These data ($t = 0$) are then mapped onto the depth section at z, the depth of extrapolation. This mapping process is also referred to as imaging. Since imaging is a standard procedure, migration schemes differ from each other in their approach to wave extrapolation, the complexity of which depends largely on the migration velocity function.

If the migration velocity has no horizontal dependence, the extrapolation of zero-offset seismic data can be expressed by the exact wave-extrapolation equation (26) in the wavenumber–frequency domain. This equation has a simple analytic solution, whose implementation calls for a phase shift applied to the Fourier coefficients of the zero-offset section. In the presence of lateral velocity variations, the exact wave-extrapolation equation (26) is no longer valid. To circumvent this problem, the exact expression can be approximated by truncated series expansions [16], [18], which can accommodate horizontal velocity variations. These equations are then solved numerically, either in the space–time domain or in the space–frequency domain.

A. Migration in the (k_x, ω) Domain

Letting $p(x, t, z = 0)$ represent the zero-offset section and $P(k_x, \omega, z = 0)$ its double Fourier transform, the wave-extrapolation equation (26) becomes

$$\frac{\partial P}{\partial z} = \frac{2i\omega}{v}\left[1-\left(\frac{k_x v}{2\omega}\right)^2\right]^{1/2}P. \quad (27)$$

The problem is to reconstruct the wavefield $p(x, t = 0, z)$, which existed at $t = 0$ from the wavefield $p(x, t, z = 0)$ observed at $z = 0$. We shall assume that within one extrapolation step, say from depth z to $z + \Delta z$, the velocity is constant, i.e.,

$$v(\zeta) = \textit{constant}, \qquad z \leqslant \zeta < z + \Delta z. \quad (28)$$

Then the solution of (27) can be expressed as

$$P(k_x, \omega, z+\Delta z) = P(k_x, \omega, z) \cdot \exp\left\{\frac{2i\omega}{v}\left[1-\left(\frac{k_x v}{2\omega}\right)^2\right]^{1/2}\Delta z\right\} \quad (29)$$

in which $P(k_x, \omega, z)$ is the zero-offset section extrapolated to depth z. This analytic solution states that P is extrapo-

lated from z to $z + \Delta z$ by simply rotating its phase by a specified amount. Therefore, migration schemes based on this principle are referred to as *phase-shift* methods [19], [20]. From $P(k_x, \omega, z)$ we obtain $p(x, t = 0, z)$ by inverse Fourier transform with respect to k_x and a summation with respect to ω, i.e.,

$$p(x, t = 0, z) = \sum_{k_x} \sum_{\omega} P(k_x, \omega, z) \exp(ik_x x). \quad (30)$$

Although (29) is valid only under the assumption expressed in (28), the velocity can vary from one Δz step to another. Thus the phase-shift method can accommodate media with vertical velocity variations, i.e., in which $v = v(z)$.

Under certain circumstances, it may be acceptable to migrate with a velocity that is constant over the entire domain (object plane) of interest. This uniform migration velocity assumption, if properly exploited, enables one to develop a very efficient migration algorithm. This migration scheme, often referred to as the *F-K method*, was first reported by Stolt [21]. Essentially, it is a fast "direct" method for the evaluation of (29) and (30). Let us rewrite (29) using z and $z = 0$ in place of $z + \Delta z$ and z, respectively, i.e.,

$$P(k_x, \omega, z) = P(k_x, \omega, z = 0) \exp(ik_z z) \quad (31)$$

where

$$k_z = \frac{2\omega}{v}\left[1 - \left(\frac{k_x v}{2\omega}\right)^2\right]^{1/2} \quad (32)$$

which represents the dispersion relations of the one-directional wave equation (27). The migrated section $p(x, t = 0, z)$ can be obtained from $P(k_x, \omega, z = 0)$ as follows:

$$p(x, t = 0, z) = \int\int d\omega\, dk_x P(k_x, \omega, z = 0) \cdot \exp\{i[k_z(\omega) z + k_x x]\} \quad (33)$$

which corresponds to (30), except that the summations are replaced by integrations. In order to take advantage of the fast Fourier transform (FFT) algorithm, we want to integrate (33) with respect to k_z instead of ω. Using (32) we can rewrite (33) as

$$p(x, t = 0, z) = \int\int dk_z\, dk_x \hat{P}(k_x, k_z) \exp\{i[k_z z + k_x x]\} \quad (34)$$

where

$$\hat{P}(k_x, k_z) = \frac{v k_z}{2[k_x^2 + k_z^2]^{1/2}} P(k_x, \omega, z = 0). \quad (35)$$

In summary, the F-K method consists of three steps:

1) the Fourier transformation of $p(x, t, z = 0)$ to obtain $P(k_x, \omega, z = 0)$,
2) the interpolation and scaling of the Fourier coefficients as expressed in (35),
3) the inverse FFT of the interpolated results as expressed in (34).

Migration with this fast method is limited to homogeneous media with constant velocity. To overcome this limitation, Stolt [21] suggested coordinate transformations to cast the wave equation in a form that is approximately velocity invariant.

B. Migration in the (x, ω) Domain

As we have seen, in the absence of horizontal velocity dependence, the set of independent ordinary differential equations (27) governs the extrapolation of the zero-offset seismic data in the (k_x, ω) domain. The simple analytic solution expressed by (29) is not valid for velocity fields with lateral variations. In this case, the square-root expression in (27) must be approximated in some form, for instance, by a quadratic polynomial (Claerbout's [22] *parabolic* approximation). The expansion can then be formally converted into a numerical method in the (x, ω) domain. After the approximation, the velocity v is allowed to vary with x as well as with z, and a wave-extrapolation equation for general media is obtained.

Another alternative is rational approximation by truncated continued fractions [23]. In this latter approach, an approximation of (27) is

$$\frac{\partial P(k_x, \omega, z)}{\partial z} = \left(\frac{2i\omega}{v}\right)\left\{1 - \frac{\frac{v^2}{4\omega^2} k_x^2}{2 - \frac{v^2}{8\omega^2} k_x^2}\right\} P(k_x, \omega, z). \quad (36)$$

A practical approach to solving extrapolation equations like (36) is by Marchuk splitting. This is done by decomposing (36) into two extrapolators

$$\frac{\partial P}{\partial z} = \left(\frac{2i\omega}{v}\right) P \quad (37)$$

which is known as the *thin lens* term, and

$$\frac{\partial P}{\partial z} = \left[\frac{-i(v/4\omega) k_x^2}{1 - (k_x v/4\omega)^2}\right] P \quad (38)$$

which is the *Fresnel diffraction* term. Advancing to greater depths is done by applying (37) and (38) alternately in small Δz steps. Equation (38) can be expressed in the (x, ω) domain first eliminating fractions and then Fourier transforming it with respect to k_x. The result is

$$\left[1 + \frac{v^2 \partial^2}{16\omega^2 \partial x^2}\right] \frac{\partial P(x, \omega, z)}{\partial z} = \left(\frac{iv}{4\omega}\right) \frac{\partial^2 P(x, \omega, z)}{\partial x^2}. \quad (39)$$

At each step Δz, (37) advances P through the multiplication by a phasor corresponding to a shift backward in time of magnitude $\Delta T = 2\Delta z / v$. To advance P with (39), for numerical stability considerations, an implicit Crank–Nicolson difference scheme is most often used.

The approximation of the square-root operator in (27) with the rational operator appearing in (36) and the finite-difference implementation of (39) alter the dispersion relations of the wave equation and generate numerical errors increasing with the expansion parameter $\sin\vartheta = vk_x/2\omega$, where ϑ represents the angle with respect to the vertical axis of the wavefront under consideration. When the dip of the imaging wavefield exceeds 40°–45°, dispersion effects separate the low frequencies from the high frequencies during the wavefront depropagation. As a result, the image of steeply dipping reflectors may be accompanied by "ghosts." The phenomenon is demonstrated through a numerical example, the model of which is

depicted in Fig. 11. The synthetic zero-offset section of the model is shown in Fig. 12. The migrated depth section obtained by a finite-difference implementation of (37) and (39) is illustrated in Fig. 13. Note that the non-steeply dipping events are clear, but the steeply dipping event has "ghosts."

Better dispersion properties can be obtained including higher order terms in the formal expansion [16]. An alternative approach to wavefield extrapolation in general media is described in [24]. At each Δz step, the wave extrapolation is accomplished in two stages. In the first stage the wavefield $P(x, \omega, z)$ given at depth z is extrapolated to $z + \Delta z$ by the phase-shift method using ℓ reference velocities $v_1, v_2, \cdots, v_\ell$ spanning the velocity range at depth z. This stage generates

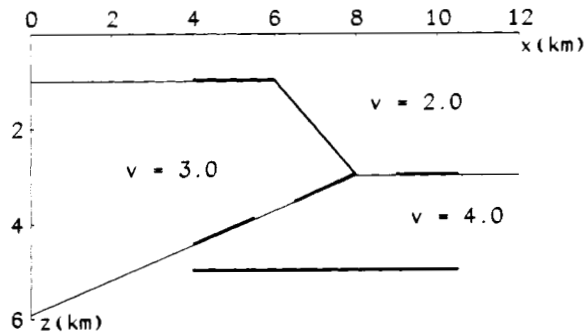

Fig. 11. Schematic of model 2, representing a dipping multilayer example. The thick-line segments indicate where the reflector segments have been "turned on."

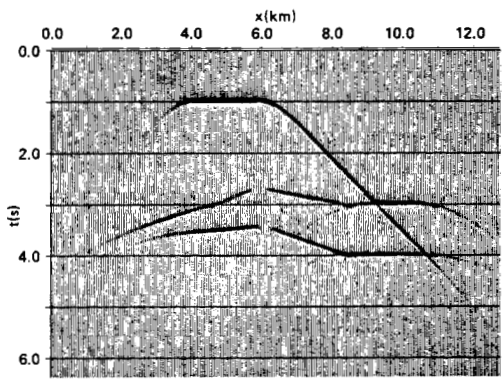

Fig. 12. Zero-offset time section of model 2.

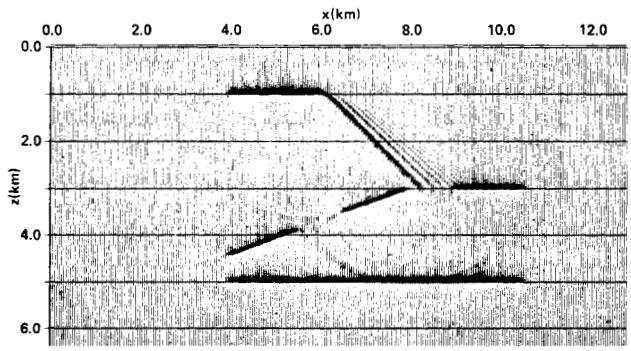

Fig. 13. Depth migration obtained from the zero-offset time section of model 2 shown in Fig. 12. The (x, ω) domain finite-difference migration method used in this example corresponds to (37) and (39). Note that the steeply dipping reflector is not imaged correctly.

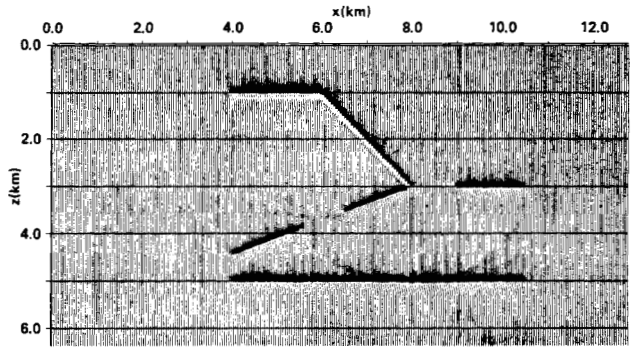

Fig. 14. Depth migration section obtained from the time section shown in Fig. 12 using the phase shift plus interpolation method. All reflectors are migrated correctly.

ℓ reference extrapolated wavefields at $z + \Delta z$, namely, $P_1, P_2, \cdots, P_\ell$. In the second stage, the definitive wavefield $P(x, \omega, z + \Delta z)$ is constructed by interpolation of the ℓ reference wavefields. This phase shift plus interpolation (PSPI) method is unconditionally stable and has good dispersion relation properties worth its relatively high computational cost (for each frequency ω, and for each step in depth, $\ell + 1$ Fourier transforms in the x direction are required). The synthetic zero-offset section of Fig. 12 migrated with the PSPI method is shown in Fig. 14. One can notice significant improvement in the migration of the steeply dipping reflector in comparison with the one shown in Fig. 13.

C. Migration in the (x, t) Domain

Migration as a wave depropagation process is best described in the "transformed" domains (k_x, ω) and (x, ω). It was introduced, however, in the early 1970s using paraxial wave equations in the "physical" space–time (x, t) [22], [14]. We will reproduce here those equations, deriving them from their frequency-domain counterparts.

An inverse Fourier transform of the wavefield $P(x, \omega, z)$ in (37) and (39) results in the following two equations in terms of $p(x, t, z)$:

$$\frac{\partial p}{\partial z} = \frac{2}{v} \frac{\partial P}{\partial t} \tag{40}$$

$$\frac{\partial^3 p}{\partial t^2 \partial z} + \frac{v}{4} \frac{\partial^3 p}{\partial x^2 \partial t} = \frac{v^2}{16} \frac{\partial^3 p}{\partial x^2 \partial z}. \tag{41}$$

For gentle dips, the right-hand side of (41) can be neglected, and it becomes

$$\frac{\partial^2 p}{\partial t \partial z} + \frac{v}{4} \frac{\partial^2 p}{\partial x^2} = 0. \tag{42}$$

Equations (40) and (41) or (40) and (42) are specialized wave equations that depropagate wave energy only within a small angle about the vertical axis, hence are called *paraxial* approximations: details on their numerical integration with finite-difference methods can be found in [12, pp. 211–212].

Seismic interpreters often find it useful to work with subsurface migrated sections with depth measured in units of time, for ease of comparison with unmigrated CMP sections. Such maps are obtained by introducing a pseudo-depth τ (vertical travel time) which is related to true depth z by

$$\tau(z) = 2\int_0^z \frac{d\zeta}{\bar{v}(\zeta)} \tag{43}$$

where $\bar{v}(z)$ is an approximation, independent of x, of the velocity $v(x,z)$. With the introduction of the vertical coordinate τ and the help of an additional approximation, (40) and (42) become

$$\frac{\partial p}{\partial \tau} = \frac{\partial p}{\partial t} \tag{44}$$

$$\frac{\partial^2 p}{\partial t \partial \tau} + \frac{\bar{v}^2}{8}\frac{\partial^2 p}{\partial x^2} = 0. \tag{45}$$

Wavefield extrapolation with (44) and (45) lead to *time migration* as opposed to *depth migration* obtained with (40) and (42). Time migration schemes depropagate the wavefield as if the medium were horizontally layered and do not correctly refract rays at the velocity interfaces, but constitute a viable and economic tool in most practical situations. An excellent example of finite-difference (time) migration of a CMP stack section is illustrated in Figs. 15 and 16. Notice the decrease in width of the diffractions on

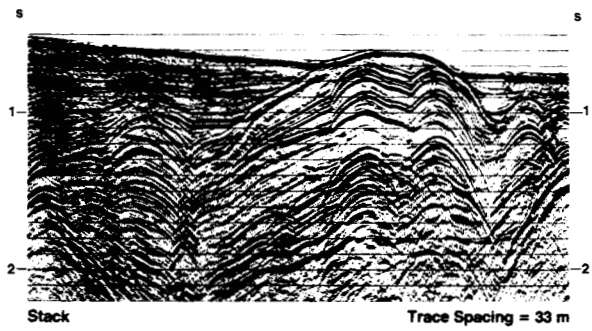

Fig. 15. CMP stacked section from data recorded in the Santa Barbara channel. Steepest dips are approximately 25°. (From Hatton *et al.* [17]; courtesy of Western Geophysical.)

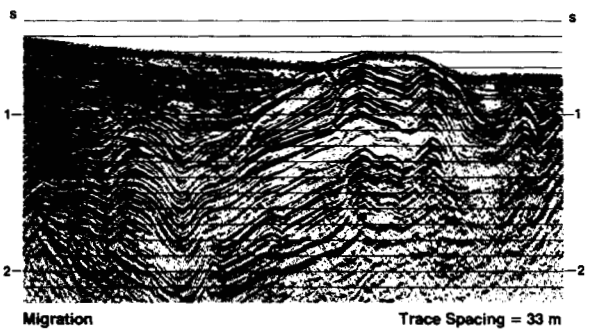

Fig. 16. Finite-difference time migration of the CMP section illustrated in Fig. 15. (From Hatton *et al.* [17]; courtesy of Western Geophysical.)

the right hand of the migrated section and the development of synclines at the left. When a better positioning is required, after time migration, a correction is made using Hubral's *image ray* time-to-depth conversion, [25, p. 103], [26], [27]. The solution of (44) can be written as $p(x,t,\tau + \Delta\tau) = p(x,t+\Delta\tau,\tau)$ which represents a uniform translation of the wavefield p along the negative t axis as τ increases. There is no need to perform this time shift explicitly. Equation (44) can be accounted for by imaging the data at $t = \tau$, rather than at $t = 0$. Time migration methods based on this imaging principle are often described as being solved in a "downward moving" coordinate frame.

VI. Wave-Equation Migration in Object Space

Migration of zero-offset data $p(x,t,z=0)$ is accomplished by the methods described in Sections IV and V through a *downward extrapolation* of surface data. Advancing in depth, image plane sections $p(x,t,z=\text{const})$ are computed and the final migrated section is given by the extrapolated wavefield at time zero $p(x,t=0,z)$. An alternative approach calls for a *reverse-time extrapolation* of the wavefield using the CMP section as a boundary condition. Marching backward in time, object plane sections (time-slices) $p(x,t=\text{const},z)$ are computed. Calculations begin at time T, which defines the last sample of the record section, and continue in the negative t direction until time zero. At that time the amplitudes in object space are considered as the final migrated section.

In this section, dealing with reverse-time migration, for the sake of clarity, we shall deviate slightly from the notations used throughout this paper. We shall let $q(x,t)$ represent the stacked CMP data, and $p(x,t,z)$ the wavefield. Consequently, $p(x,t=0,z)$ will represent the migrated CMP section.

In object space, just as in image space, migration schemes differ from each other only in the type of wave equations being used for wave extrapolation. For example, Hemon [28] and McMechan [29] suggested the "full" wave equation

$$\frac{\partial^2 p}{\partial t^2} = \left(\frac{v}{2}\right)^2\left[\frac{\partial^2 p}{\partial x^2} + \frac{\partial^2 p}{\partial z^2}\right] \tag{46}$$

which corresponds to our (8) or (9) expressed in the midpoint variable x. This equation is then integrated numerically with the following initial conditions:

$$p(x,t=T,z) = 0, \qquad \text{for } z \neq 0 \tag{47}$$

and

$$\frac{\partial p}{\partial t}(x,t=T,z) = 0. \tag{48}$$

The boundary conditions at the surface are given by

$$p(x,t,z=0) = q(x,t). \tag{49}$$

The problem with (46) is that it allows for reflections from interfaces where the velocity changes rapidly. We recall that the exploding reflector model shown in Fig. 4 assumes that the surface record includes only upward propagating waves. Therefore, in the *depropagation* phase all wave components should move downward in reverse time, and no upward reflected waves are admissible. This problem can be easily avoided if one uses, instead of (46), a one-directional wave equation. Baysal *et al.* [30] and Loewenthal *et al.* [31] used an equation for downward propagating waves

$$\frac{\partial p}{\partial t} = \frac{v}{2}\left\{\mathcal{F}^{-1} ik_z\left[1 + (k_x/k_z)^2\right]^{1/2}\mathcal{F}\right\}p \tag{50}$$

where $\mathcal{F}$ and $\mathcal{F}^{-1}$ are operators representing the double Fourier transform from the (x,z) domain to the (k_x,k_z) domain and its inverse. Unfortunately, (50) cannot be written without the transform operators $\mathcal{F}$ and $\mathcal{F}^{-1}$, since the multiplication in the Fourier space by $ik_z[1 + (k_x/k_z)^2]^{1/2}$

cannot be expressed in the (x,z) space. Further details regarding (50) and its numerical solution are found in [32] and [33]. The initial and boundary conditions for reverse-time migration with (50) are given by (47) and (49), respectively. Using a third-order Runge–Kutta algorithm, for example, to solve (50) on the zero-offset section shown in Fig. 12 generates the migrated depth section illustrated in Fig. 17.

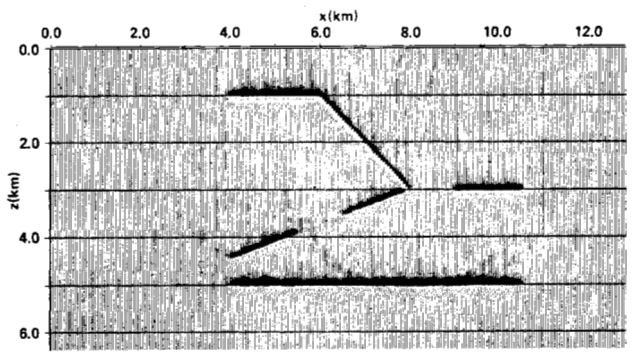

Fig. 17. Depth migration section obtained from the time section shown in Fig. 12 using reverse-time migration based on (50).

Another approach to reducing reflections was reported by Baysal *et al.* [35], who propose the use of a two-way nonreflecting wave equation. Their approach begins considering the general wave equation [34, p. 171]

$$\frac{\partial^2 p}{\partial t^2} = \left(\frac{v}{2}\right)^2 \left\{ \rho \frac{\partial}{\partial x}\left[\frac{1}{\rho}\frac{\partial p}{\partial x}\right] + \rho \frac{\partial}{\partial z}\left[\frac{1}{\rho}\frac{\partial p}{\partial z}\right] \right\} \qquad (51)$$

where ρ is the density of the medium. Since ρ does not play any role in migration, its value may be chosen to minimize reflection. This is done by setting ρ so that the acoustic impedance

$$K(x,z) = \rho(x,z)\, v(x,z) = \text{constant} \qquad (52)$$

over the entire object plane.

The basic concept of using CMP data as a boundary condition and computing its "response" in the object plane is not new. The heuristic method called wavefront interference migration discussed in Section III is based on the same principle. The only important difference is that the reverse-time migration methods are based on a wave-equation solution rather than the intuitive approach depicted in Fig. 8.

VII. Migration Before Stacking

The task of imaging the subsurface in conventional seismic data processing is partitioned in two steps: the *stacking* of the CMP gathers, and the *migration* of the CMP stacked section. This procedure, however, is correct only for a simplified subsurface model consisting of horizontal layers of laterally uniform velocity and of horizontal reflectors. Levin [36] has shown that the stacking velocity depends not only on the propagation velocity of the overburden but also on the dip angle of the reflectors. In structurally complex formations, the correction for all dip angles becomes impossible, and stacking loses its effectiveness. Under these circumstances, it may be advantageous to consider *migration before stacking*.

The theoretical basis for migration of unstacked (multioffset) data was discussed in Section IV. In this process, the multioffset data are converted (see, for example, (17) and (21)) into a migrated zero-offset section. This is a relatively costly process and does not provide any intermediate results. To overcome these shortcomings of the "one-step" migration of unstacked data, a number of special-purpose before-stack migration techniques were developed. For example, the *prestack partial migration* [15] and the *offset continuation* algorithm [37], [38] are applied to common-offset sections after they have been NMO corrected. These *stack-enhancement* [39] techniques share the advantage of yielding an unmigrated CMP stack section that helps the interpreter in resolving spurious events generated on the final migrated section by inaccurate velocity estimates. They are computationally more expensive than the conventional processing since they introduce an additional process between NMO and stacking but leave the migration cost unchanged.

The methods described in this section belong to the former category in which the separate components of the conventional processing (NMO, stacking, zero-offset migration) are merged into a unified process. They represent the best methods available for imaging the subsurface in a variable velocity medium. They are, unfortunately, also the most expensive in terms of computation and data handling.

A. Migration of Multioffset Data

The theoretical considerations for migration of multioffset data were presented in Section IV. The wavefield extrapolation is governed by (17), and the imaging is accomplished by implementing (21). The solution by phase shift of (17), expressed by (18), can accommodate only vertical velocity variations from one Δz step to another. In the presence of lateral velocity variations, (17) needs to be generalized as follows [15]:

$$\frac{\partial P}{\partial z} = i\omega \left\{ \frac{1}{v(r,z)}\left(1-\kappa_r^2\right)^{1/2} + \frac{1}{v(s,z)}\left(1-\kappa_s^2\right)^{1/2} \right\} P \qquad (53)$$

where κ_r and κ_s are given by (14). This implies that we distinguish between the velocity along the shot axis and the velocity along the shot axis and the velocity along the receiver axis. We hasten to point out, however, that in (53) the algebraic expressions in the operators κ_r and κ_s are not immediately defined when $v(r,z)$ and $v(s,z)$ have lateral variations. This is the same limitation as the one we have encountered with the single-square-root equation (27). Fortunately, most of the solution methods for zero-offset migration are applicable to (53). In other words, multioffset data can be extrapolated by the PSPI method or by finite-difference methods developed in the (r,s,ω) domain or in the (r,s,t) domain.

Having decided on a suitable extrapolation scheme, before-stack migration can be summarized as follows [40]. The algorithm operates on the entire data volume $p(r,s,t,z=0)$ processing it in the alternating directions r and s. For each depth level z, in increments of Δz, beginning with $z=0$, the following steps are executed:

1) Order the data into common-shot gathers $p(r,s_0,t,z)$ and extrapolate downward from z to $z+\Delta z$ each common-source gather $s=s_0$ using (12).

2) Reorder the data obtained from step 1 into common-

receiver gathers $r = r_0$ and extrapolate downward by Δz each common-receiver gather $r = r_0$ using (13).

3) Perform the imaging $m(x,z) = p(r = x, s = x, t = 0, z)$, where $m(x,z)$ is the migrated CMP section.

B. Migration of Common-Shot Gathers

Migration before stacking can also be accomplished by migrating the individual common-shot gathers and summing these migrated gathers. The downward extrapolation of the recorders is governed by (12) or some approximation thereof. The extrapolated wavefield is focused at the reflector location, not at time zero, but at the propagation time between the shot and the reflector. To simplify matters, let us consider a single point reflector, for example P_1 in Fig. 2, whose position (r', z') is specified in the receiver–depth coordinate system. The event corresponding to the point reflector P_1 is observed at $t = t_1 + t_2$, where $t_1(s; r', z')$ is the travel time between the source and the reflector, and $t_2(r; r', z')$ is the travel time between the reflector and the receiver. Under these assumptions, the downward extrapolation focuses the recorded wavefield in the neighborhood of the point (r', z') at time $t_1(s; r', z')$, which is the correct time for imaging.

We are now in a position to set forth an algorithm for migration before stack. For each common-shot gather $p(r, \bar{s}, t, z = 0)$ we execute the following steps:

1) Compute the arrival time of the primary wavefield $t_1 = t_1(\bar{s}; r', z')$ at all points (r', z') of the subsurface.

2) Extrapolate downward (for instance with (12)) in depth the common-shot data $p(r, \bar{s}, t, z = 0)$, thus regenerating for each point of the subsurface the scattered field $p(r', \bar{s}, t, z')$.

3) Perform the imaging

$$m(r', z'; \bar{s}) = p\big(r', \bar{s}, t_1(\bar{s}; r', z'), z'\big). \tag{54}$$

Then sum over a set of migrated common-source gathers, that is,

$$m(r', z') = \sum_{\bar{s}} m(r', z'; \bar{s}). \tag{55}$$

The procedure is illustrated in the following example. Fig. 18 shows a model consisting of four layers separated by reflecting interfaces: the velocity of the medium ranges from 2.0 to 3.5 km/s. Fig. 19 shows the common-shot gather that is obtained setting $s = 1.5$ km. There are 96 traces with a spacing of $\Delta x = 25$ m, the sampling time is $\Delta t = 10$ ms, and 256 samples define a trace. Finally, Fig. 20

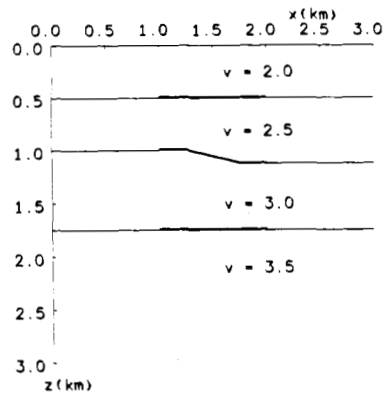

Fig. 18. Schematic of model 3, representing a multilayer example with a gentle dip in the second reflector. The thick-line segments denote reflectors.

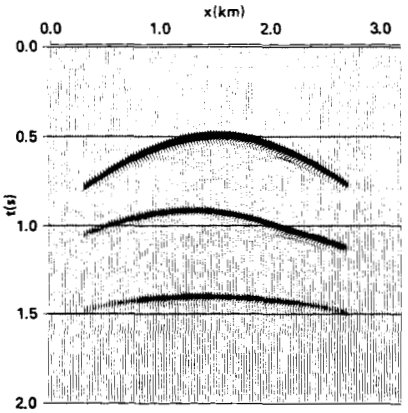

Fig. 19. A synthetic common-shot gather obtained from model 3 with source location $s = 1.5$ km.

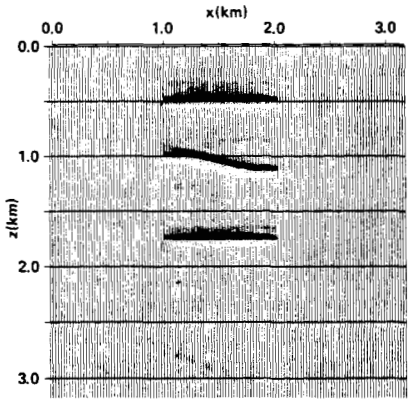

Fig. 20. Depth section obtained by migration before stack. First, the common-source gathers of model 3 with source locations ranging from 1 to 2 km are migrated. The section shown is the result of the superposition of 40 migrated gathers.

shows the superposition of 40 migrated common-shot gathers spanning the interval between $s = 1$ km and $s = 2$ km.

C. Relative Merits of the Two Approaches

The treatment of the multioffset seismic data in the source–receiver coordinate system, as described above, has a rather good theoretical foundation. Unfortunately, it involves very large amounts of data, the repeated transfer of which from primary storage to secondary storage, together with the necessary data transpositions, can become rather burdensome and taxing on the computing system. The migration of individual common-shot gathers, on the other hand, requires relatively little storage space and the computations are simpler in comparison with the former approach, which call for the simultaneous migration of a large set of common-shot gathers. The only serious problem for which one must be prepared is related to imaging. The imaging of the extrapolated wavefield, expressed by (54), requires the knowledge of the arrival time of the primary wavefield. So long as this arrival time $t_1(s; r, z)$ is a single-valued function of r and z, there is no problem. If, however, there are multiple raypaths between the source s and some points of the (r, z) domain, t_1 may assume multiple values, and there is no longer a uniquely defined imaging time. In this case, following [14], the primary wavefield must also be com-

puted and the imaging must be performed deconvolving the scattered wavefield by the primary wavefield.

VIII. Concluding Remarks

We have presented an overview of the major advances in seismic migration. Our aim was to provide a logical sequence of development rather than a historical one. We have put emphasis on the fundamental concepts of migration and have carefully avoided passing judgement or appraising value based upon their current populatiry. The merit of a migration method is largely decided by economic factors. These factors change rapidly with the advancement of recording technology, computer architecture, and cost–performance indices of data processing systems.

Mainly for reasons of cost, migration in the 1970s was applied to stacked CMP sections, and lateral velocity changes were not correctly taken into account in routine migration programs. With the continuing trend toward lower cost–performance ratio in advanced computer architectures, high-accuracy migration methods can be expected to gain acceptance in the near future. Another area that will receive increased attention is migration before stacking. In addition to better migration, a major benefit resulting from migration before stacking can be derived from improved velocity information. Ideally, we would like to have a process that simultaneously images velocities and migrates data to correct subsurface locations. This calls for imaging part of the subsurface recursively step by step, using migration and velocity analysis procedures [41], [42].

Seismic exploration methods and processing techniques are growing rapidly. Innovations can be observed over a broad range from recording techniques to displays. Recording techniques have been developed to provide areal coverage. Acquisition and migration of seismic data in three dimensions are becoming widespread. These methods are particularly useful in the presence of complex structures. Migration algorithms for three-dimensional data are natural extensions of those used for two-dimensional data [43], [44].

Increasing demand for oil and decreasing availability of hydrocarbon deposits are the motivating forces behind most innovative techniques which have one thing in common: they are aimed at improving resolution. A decade ago, geophysicists might have been satisfied with mapping the gross structure of the subterrain. Today, they hope to determine rock parameters, hydrocarbon content, as well as entrapment structure. These demands have stimulated research in more general and theoretically appealing inverse methods [45]–[52]. These works, when developed into practical processing tools, have the potential of providing insight into long-standing unsolved geophysical problems.

Acknowledgment

The authors wish to thank B. Gibson of Western Geophysical Company for providing Figs. 15 and 16.

References

[1] D. Loewenthal, L. Lou, R. Robertson, and J. W. Sherwood, "The wave equation applied to migration," *Geophys. Prospect.*, vol. 24, pp. 380–399, 1976.

[2] J. G. Hagedoorn, "A process of seismic reflection interpretation," *Geophys. Prospect.*, vol. 2, pp. 85–127, 1954.

[3] J. D. Johnson and W. S. French, "Migration—The inverse method," in *Concepts and Techniques in Oil and Gas Exploration*, K. C. Jain and R. J. P. de Figueiredo, Eds. Tulsa, OK: Soc. Exploration Geophysicists, 1982, pp. 115–157.

[4] W. A. Schneider, "Developments in seismic data processing and analysis: 1968–1970," *Geophys.*, vol. 36, pp. 1043–1073, 1971.

[5] M. Born and E. Wolf, *Principles of Optics*, 3rd ed. New York: Pergamon, 1965.

[6] W. S. French, "Computer migration of oblique seismic reflection profiles," *Geophys.*, vol. 40, pp. 961–980, 1975.

[7] W. A. Schneider, "Integral formulation for migration in two and three dimensions," *Geophys.*, vol. 43, pp. 49–76, 1978.

[8] A. J. Berkhout, *Seismic Migration.* Amsterdam, The Netherlands: Elsevier 1980.

[9] A. J. Berkhout, "Wave field extrapolation techniques in seismic migration, a tutorial," *Geophys.*, vol. 46, pp. 1638–1656, 1981.

[10] J. A. Carter and L. N. Frazer, "Accomodating lateral velocity changes in Kirchhoff migration by means of Fermat's principle," *Geophys.*, vol. 49, pp. 46–53, 1984.

[11] G. H. F. Gardner, W. S. French, and T. Matzuk, "Elements of migration and velocity analysis," *Geophys.*, vol. 39, pp. 811–825, 1974.

[12] J. F. Claerbout, *Fundamentals of Geophysical Data Processing.* New York: McGraw-Hill, 1976.

[13] E. A. Robinson and M. T. Silvia, *Digital Foundations of Time Series Analysis: Vol 2, Wave Equation Space Time Processing.* San Francisco, CA: Holden-Day, 1981.

[14] J. F. Claerbout, "Toward a unified theory of reflector mapping," *Geophys.*, vol. 36, pp. 467–481, 1971.

[15] O. Yilmaz and J. F. Claerbout, "Prestack partial migration," *Geophys.*, vol. 45, pp. 1753–1779, 1980.

[16] J. Gazdag, "Wave equation migration with the accurate space derivative method," *Geophys. Prospect.*, vol. 28, pp. 60–70, 1980.

[17] L. Hatton, K. L. Larner, and B. S. Gibson, "Migration of seismic data from inhomogeneous media," *Geophys.*, vol. 46, pp. 751–767, 1981.

[18] A. J. Berkhout and D. W. Van W. Palthe, "Migration in terms of spatial deconvolution," *Geophys. Prospect.*, vol. 27, pp. 261–291, 1979.

[19] J. Gazdag, "Wave equation migration with the phase-shift method," *Geophys.*, vol. 43, pp. 1342–1351, 1978.

[20] G. Bolondi, F. Rocca, and A. Savelli, "A frequency domain approach to two-dimensional migration," *Geophys. Prospect.*, vol. 26, pp. 750–772, 1978.

[21] R. H. Stolt, "Migration by Fourier transform," *Geophys.*, vol. 43, pp. 23–48, 1978.

[22] J. F. Claerbout, "Coarse grid calculation of waves in inhomogeneous media with application to the delineation of complicated seismic structures," *Geophys.*, vol. 35, pp. 407–418, 1970.

[23] R. Clayton and B. Engquist, "Absorbing boundary conditions for acoustic and elastic wave equations," *Bull. Seis. Soc. Amer.*, vol. 67, pp. 1529–1540, 1977.

[24] J. Gazdag and P. Sguazzero, "Migration of seismic data by phase shift plus interpolation," *Geophys.*, vol. 49, pp. 124–131, 1984.

[25] P. Hubral and T. Krey, *Interval Velocities from Seismic Reflection Time Measurements.* Tulsa, OK: Soc. Exploration Geophysicists, 1980.

[26] P. Hubral, "Time migration—Some ray theoretical aspects," *Geophys. Prospect.*, vol. 25, pp. 738–745, 1977.

[27] K. L. Larner, L. Hatton, B. S. Gibson, and I-C. Hsu, "Depth migration of imaged time sections," *Geophys.*, vol. 46, pp. 734–750, 1981.

[28] C. Hemon, "Equations d'onde et modeles," *Geophys. Prospect.*, vol. 26, pp. 790–821, 1978.

[29] G. A. McMechan, "Migration by extrapolation of time-dependent boundary values," *Geophys. Prospect.*, vol. 31, pp. 413–420, 1983.

[30] E. Baysal, D. D. Kosloff, and J. Sherwood, "Reverse time migration," *Geophys.*, vol. 48, pp. 1514–1524, 1983.

[31] D. Loewenthal and I. R. Mufti, "Reversed time migration in spatial frequency domain," *Geophys.*, vol. 48, pp. 627–635, 1983.

[32] J. Gazdag, "Extrapolation of seismic waveforms by Fourier

methods," *IBM J. Res. Develop.*, vol. 22, pp. 481–486, 1978.
[33] _____, "Modeling of the acoustic wave equation with transform methods," *Geophys.*, vol. 46, pp. 854–859, 1981.
[34] L. M. Brekhovskikh, *Waves in Layered Media*. New York: Academic Press, 1960.
[35] E. Baysal, D. D. Kosloff, and J. Sherwood, "A two-way nonreflecting wave equation," *Geophys.*, vol. 49, pp. 132–141, 1984.
[36] F. K. Levin, "Apparent velocity from dipping interface reflections," *Geophys.*, vol. 36, pp. 510–516, 1971.
[37] G. Bolondi, E. Loinger, and F. Rocca, "Offset continuation of seismic sections," *Geophys. Prospect.*, vol. 30, pp. 813–828, 1982.
[38] S. M. Deregowski and F. Rocca, "Geometrical optics and wave theory of constant offset sections in layered media," *Geophys. Prospect.*, vol. 29, pp. 374–406, 1981.
[39] P. Hood, "Migration," in *Developments in Geophysical Exploration Methods—2*, A. A. Fitch, Ed. London, England: Applied Science Publ. 1981, pp. 151–230.
[40] P. S. Schultz and J. W. C. Sherwood, "Depth migration before stack," *Geophys.*, vol. 45, pp. 376–393, 1980.
[41] P. S. Schultz, "A method for direct estimation of interval velocities," *Geophys.*, vol. 47, pp. 1657–1671, 1982.
[42] J. Gazdag and P. Sguazzero, "Interval analysis by wave extrapolation," *Geophys. Prospect.*, vol. 32, pp. 454–479, 1984.
[43] B. Gibson, K. Larner, and S. Levin, "Efficient 3-D migration in two steps," *Geophy. Prospect.*, vol. 31, pp. 1–33, 1983.
[44] H. Jakubowicz and S. Levin, "A simple exact method of 3-D migration—Theory," *Geophys. Prospect.*, vol. 31, pp. 34–56, 1983.
[45] J. K. Cohen and N. Bleistein, "An inverse method for determining small variations in propagation speed," *SIAM J. Appl. Math.*, vol. 32, pp. 784–799, 1977.
[46] _____, "Velocity inversion procedure for acoustic waves," *Geophys.*, vol. 44, pp. 1077–1087, 1979.
[47] S. Raz, "Direct reconstruction of velocity and density from scattered field data," *Geophys.*, vol. 46, pp. 832–836, 1981.
[48] R. W. Clayton and R. H. Stolt, "A Born-WKBJ inversion method for acoustic reflection data," *Geophys.*, vol. 46, pp. 1559–1567, 1981.
[49] M. Lahlou, J. K. Cohen, and N. Bleistein, "Highly accurate inversion methods for three-dimensional stratified media," *SIAM J. Appl. Math.*, vol. 43, pp. 726–758, 1983.
[50] F. G. Hagin and J. K. Cohen, "Refinements to the linear velocity inversion theory," *Geophys.*, vol. 49, pp. 112–118, 1984.
[51] A. Bamberger, G. Chavent, and P. Lailly, "About the stability of the inverse problem in 1-D wave equations—Application to the interpretation of seismic profiles," *Appl. Math. Optim.*, vol. 5, pp. 1–47, 1979.
[52] P. Lailly, "The seismic inverse problem as a sequence of before stack migrations," presented at the Conf. on Inverse Scattering, Univ. Tulsa, Tulsa, OK, May 1983.

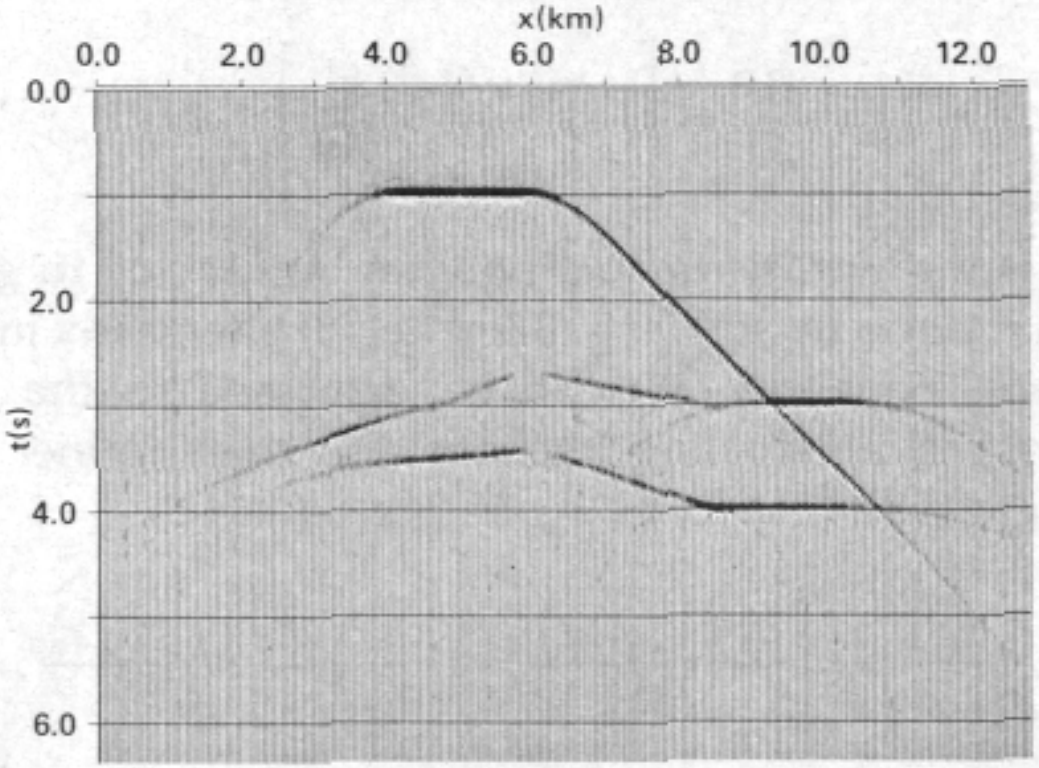

Fig. 12. Zero-offset time section of model 2.

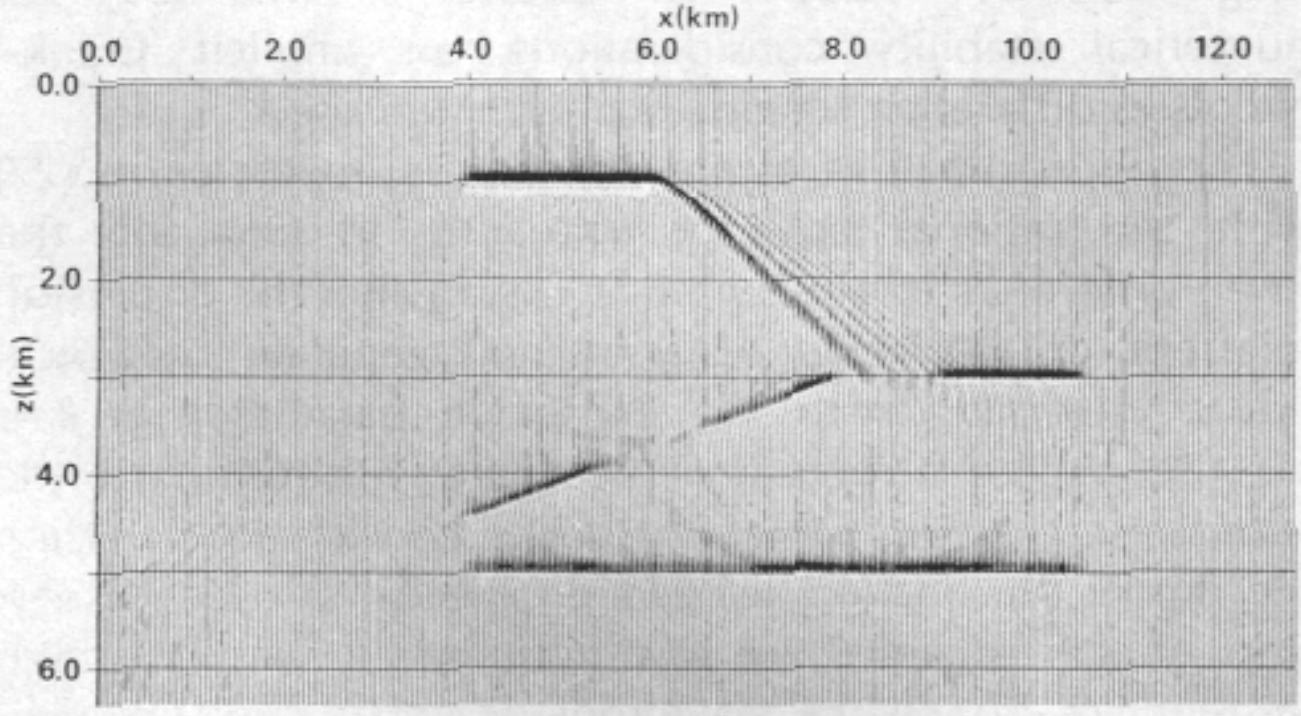

Fig. 13. Depth migration obtained from the zero-offset time section of model 2 shown in Fig. 12. The (x, ω) domain finite-difference migration method used in this example corresponds to (37) and (39). Note that the steeply dipping reflector is not imaged correctly.

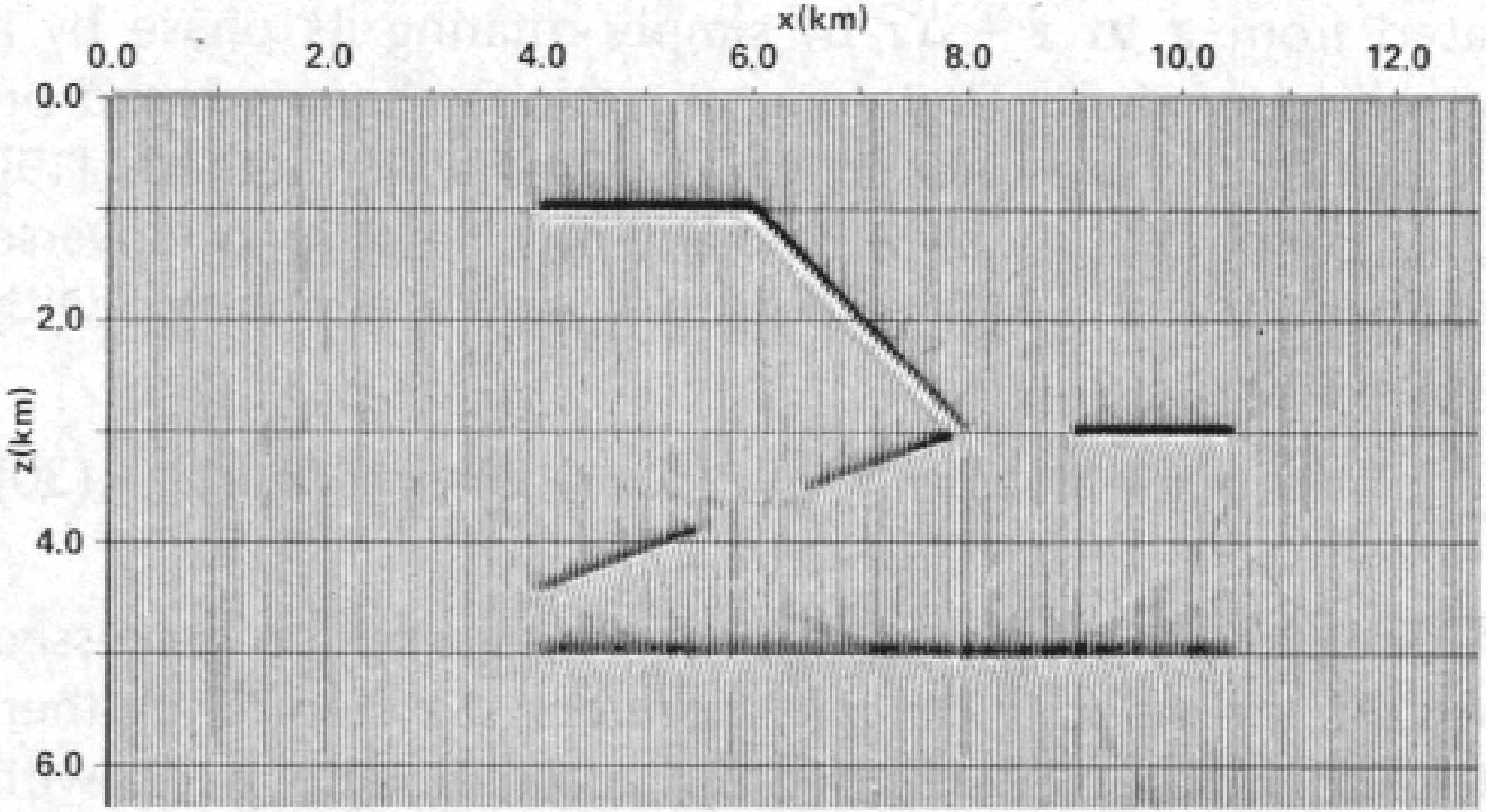

Fig. 14. Depth migration section obtained from the time section shown in Fig. 12 using the phase shift plus interpolation method. All reflectors are migrated correctly.

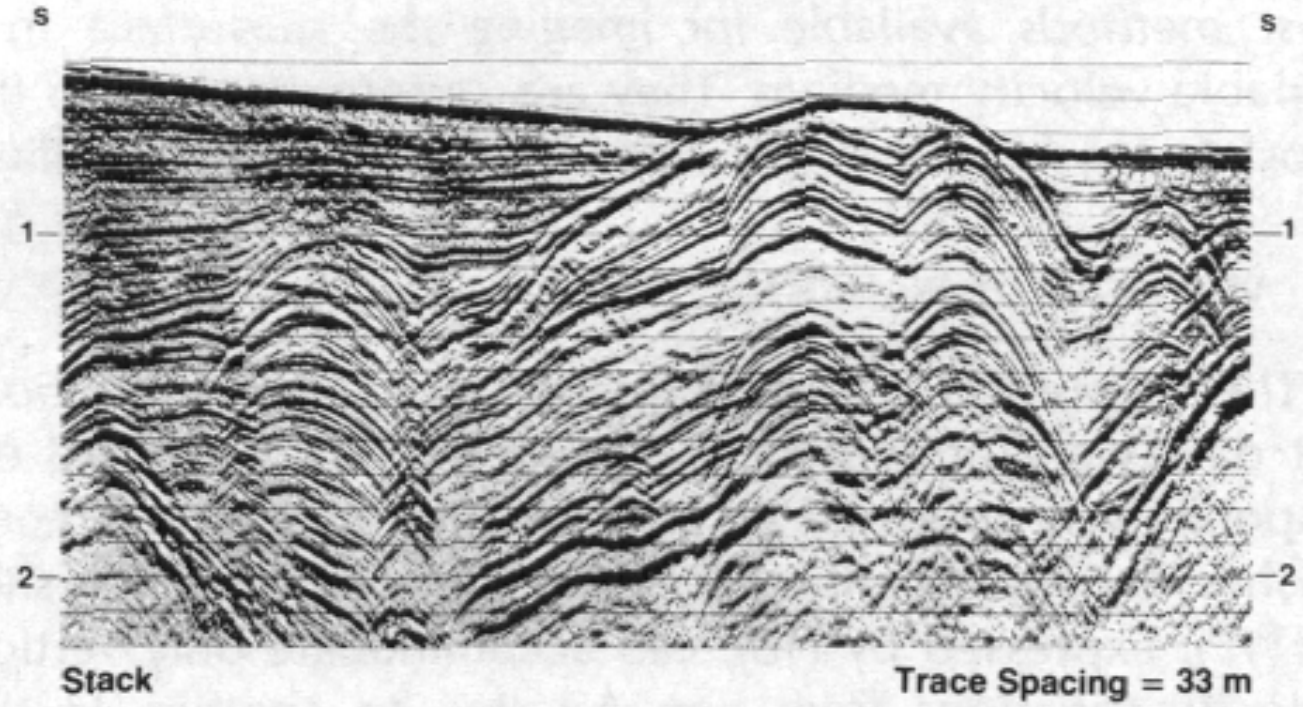

Fig. 15. CMP stacked section from data recorded in the Santa Barbara channel. Steepest dips are approximately 25°. (From Hatton *et al.* [17]; courtesy of Western Geophysical.)

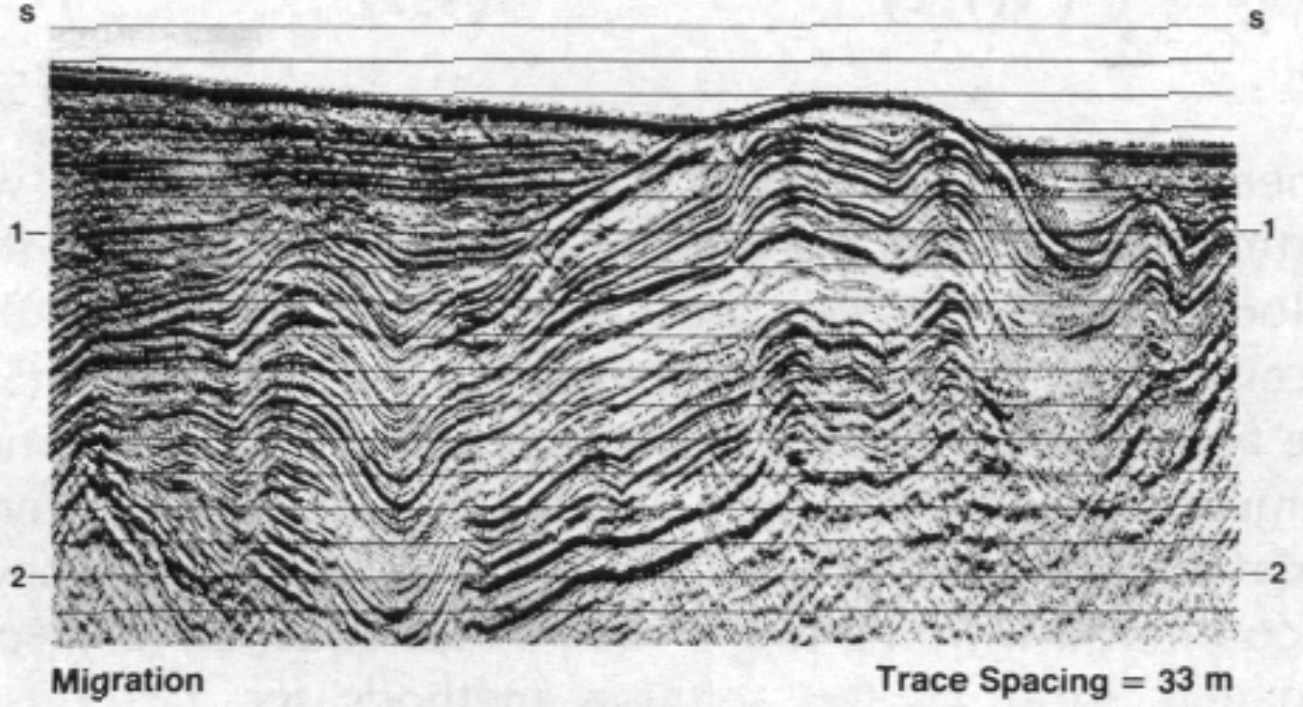

Fig. 16. Finite-difference time migration of the CMP section illustrated in Fig. 15. (From Hatton *et al.* [17]; courtesy of Western Geophysical.)

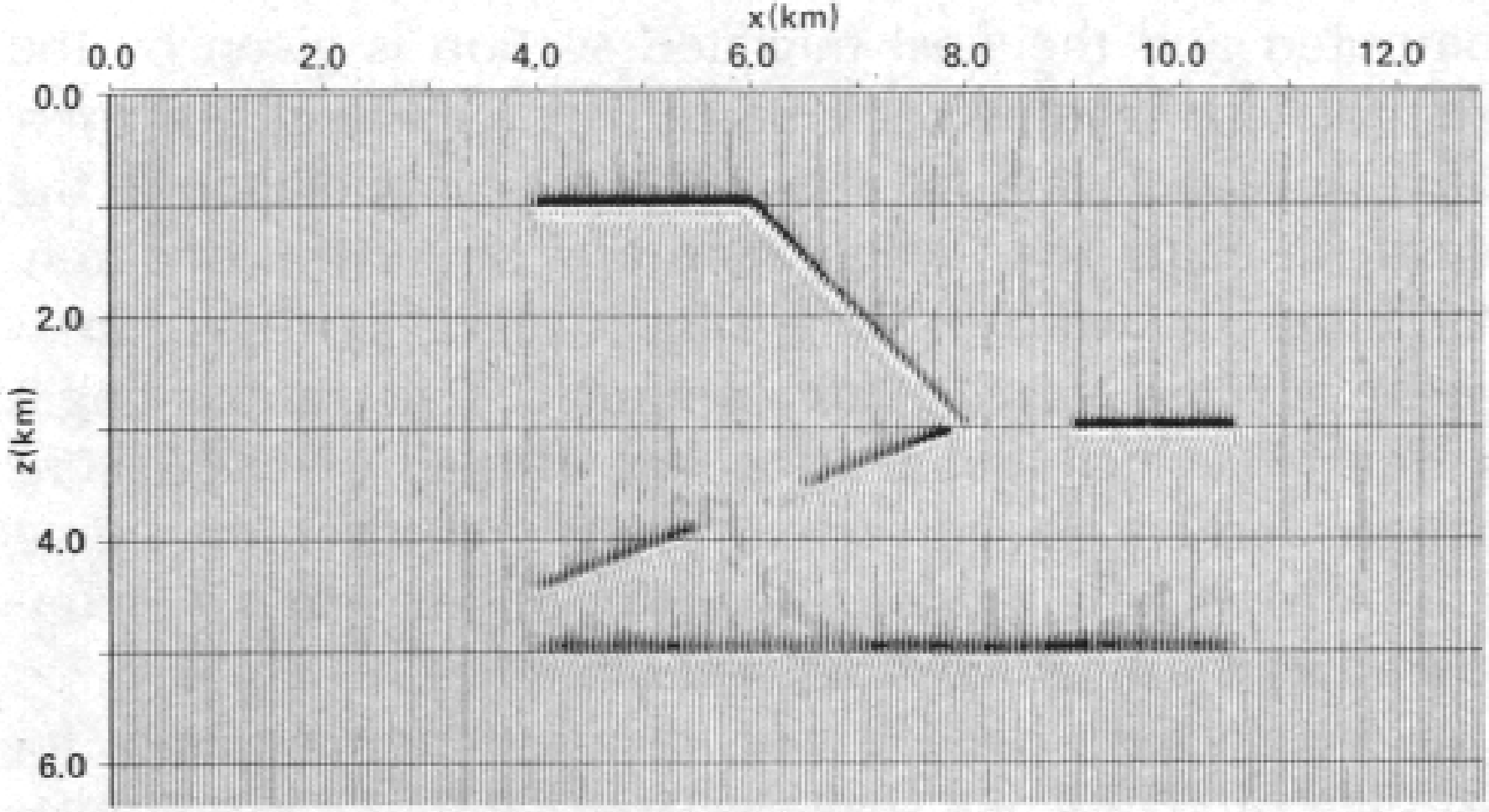

Fig. 17. Depth migration section obtained from the time section shown in Fig. 12 using reverse-time migration based on (50).

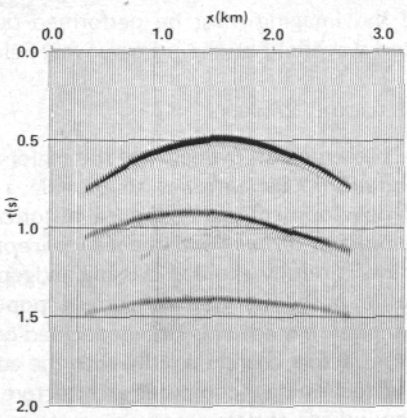

Fig. 19. A synthetic common-shot gather obtained from model 3 with source location $s = 1.5$ km.

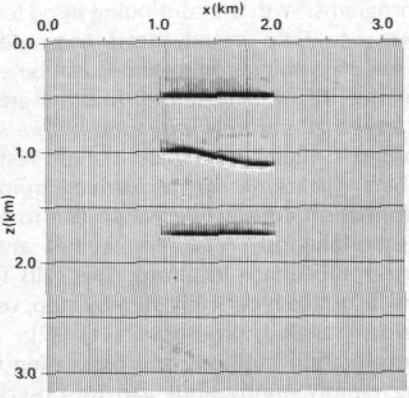

Fig. 20. Depth section obtained by migration before stack. First, the common-source gathers of model 3 with source locations ranging from 1 to 2 km are migrated. The section shown is the result of the superposition of 40 migrated gathers.